A Comparative Study of Agarose and Sodium Alginate-Based Gel Polymer Electrolytes for Zn-Based Batteries With CaV6O16·3H2O Cathode

Battery Energy

WILEY

RESEARCH ARTICLE OPEN ACCESS

A Comparative Study of Agarose and Sodium Alginate-Based Gel Polymer Electrolytes for Zn-Based Batteries With $CaV_6O_{16}{\cdot}3H_2O$ Cathode

Matteo Milanesi[1,2] | Alessandro Piovano[1,2] | Hamideh Darjazi[1,2] | Xu Liu[3] | Claudio Gerbaldi[1,2] | Giuseppe A. Elia[1,2]

[1]GAME Lab, Department of Applied Science and Technology (DISAT), Politecnico di Torino, Torino, Italy | [2]National Reference Center for Electrochemical Energy Storage (GISEL) - INSTM, Firenze, Italy | [3]School of Energy and Environment & Z Energy Storage Center, Southeast University, Nanjing, China

Correspondence: Giuseppe A. Elia (giuseppe.elia@polito.it)

Received: 3 July 2025 | **Revised:** 15 October 2025 | **Accepted:** 17 October 2025

Funding: The HIPERZAB project (https://hiperzab.eu/en) has received funding from the European Union's EIC research and innovation programme under grant agreement No 101115421. Views and opinions expressed are, however, those of the author(s) only and do not necessarily reflect those of the European Union. Neither the European Union nor the granting authority can be held responsible for them. Part of this study was carried out within the activities "Ricerca Sistema Elettrico" 2025-27 funded through contributions to research and development by the Italian Ministry of Economic Development. Support under the MUR program "Dipartimenti di Eccellenza 2023–2027" (CUPE17G22001490006) is gratefully acknowledged.

Keywords: agarose | bio-polymer | gel polymer electrolyte | sodium alginate | V-based cathode | zinc battery

ABSTRACT

Aqueous zinc-based batteries (ZIBs) are considered promising energy storage solutions, particularly targeting low-cost applications needed for levelling electricity production from renewable energy sources. However, numerous challenges need to be overcome to bring the technology to the market, chiefly including cathode dissolution, dendrite formation, hydrogen evolution reaction, and zinc corrosion. The optimisation of the electrolyte, particularly the use of gel-polymer electrolytes (GPEs), is demonstrated as a viable approach to solve or mitigate such issues. In this respect, a comparative study of two GPEs based on biopolymers, agarose and sodium alginate, is presented here. Despite the fast and facile preparation procedure, the GPEs demonstrate to be strongly effective in suppressing dendrite and byproduct formation on zinc metal anodes, due to the abundant −OH groups along the chains in polymeric matrices. The electrochemical behaviour of GPEs is evaluated in terms of galvanostatic cycling in laboratory-scale zinc metal cells with a $CaV_6O_{16}{\cdot}3H_2O$ cathode at low and high active material loadings of 2.5 and 5 mg cm^{-2}, respectively. Resulting cycling performances in terms of specific capacity and rate capability are comparable (low loading electrodes) and even outperform (high loading electrodes) those obtained with a standard liquid electrolyte (2M $ZnSO_4$) laboratory-scale cell, thus accounting for the promising prospects of the bio-polymer GPEs as an alternative green, sustainable electrolyte for next-generation Zn-based batteries.

1 | Introduction

Electrochemical energy storage plays a crucial role in addressing climate change and facilitating the green transition by enabling the efficient storage and deployment of renewable energy. Because renewable sources like solar and wind are naturally intermittent, dependable energy storage is essential to capture surplus power during peak generation and supply it when demand rises. Batteries, the preferred power source for electric vehicles, also play a vital role in renewable energy systems by offering efficient and scalable storage solutions. In this respect, rechargeable lithium-ion batteries (LIBs) are

nowadays the leading solution due to their high energy densities, low self-discharge rates, and long operational lifespans [1]. Thanks to their versatility, they can be used in a wide range of applications, from portable electronics to automotive, and large-scale storage from renewables. However, current LIBs depend on scarce, expensive, and even hazardous materials. In particular, the use of cobalt and nickel in the preparation of cathode materials is extremely critical, as well as the use of natural graphite at the anode and lithium in the whole system; while these are the primary critical raw materials (CRMs), other materials like copper, aluminium, and various electrolytes and separators are also needed in the battery manufacturing process [2].

The development of alternative electrochemical storage systems based on abundant and non-critical elements is considered a suitable solution to ease the resource concerns associated with LIB technology [3]. Energy storage systems based on more abundant elements, such as Na^+, K^+, Mg^{2+}, Ca^{2+}, Zn^{2+}, and Al^{3+} have been widely investigated in recent years, and notably, the Na-ion battery technology successfully reached the market [4, 5]. In particular, zinc (Zn), possessing a high theoretical capacity of 820 mAh g^{-1} or 5855 mAh cm^{-3}, is considered very interesting for realising low-cost and sustainable electrochemical storage systems using aqueous electrolytes, being also sustainable-by-design as they use water as the ion conducting medium [6]. The Zn^{2+}/Zn redox process takes place at a higher potential (–0.76 V vs. SHE) compared to other metals such as Mg^{2+} (–2.37 V vs. SHE), Ca^{2+} (–2.87 V vs. SHE) and Al^{3+} (–1.66 V vs. SHE), which reduces the cell operating voltage, but allows the use of water-based electrolytes with a reduced competition with the hydrogen evolution reaction (HER) side process. Using aqueous electrolytes with mild-acidic or neutral pH minimises such parasitic reactions. In addition, it brings an intrinsic enhanced safety, together with a boost in ionic conductivity, compared to organic electrolytes generally used in LIBs or NIBs. Thanks to its dielectric constant and dipolar moment, water exhibits acid–base behaviour and solvation capabilities that only this solvent has. Moreover, ion-pairing and ion triplets formation in organic electrolytes is much more severe than in aqueous electrolytes, which has detrimental effects on the rate capabilities and cycle life of the batteries [7]. For these reasons, aqueous zinc-based batteries stand out as one of the best candidates for future sustainable electrochemical energy storage systems [7, 8], including both rechargeable zinc-ion batteries (ZIBs) and primary zinc–air batteries (ZABs). ZIBs offer efficient rechargeability and are well-suited for grid-scale storage due to their intrinsic safety, ensured by aqueous electrolytes, and their environmental and economic sustainability, stemming from abundancy and low cost of zinc. Albeit offering much higher theoretical energy densities by utilising atmospheric oxygen, ZABs suffer from limited rechargeability caused by air-catalyst degradation [9]. Nevertheless, their safety, low weight, stable voltage, and low cost make them suitable for portable and emergency applications [10]. Overall, ZIBs and ZABs highlight the versatility of zinc-based systems for both stationary and portable energy storage application [11, 12].

Besides the above detailed advantages, several challenges still hinder the commercialisation of ZIBs, chiefly including the anode stability, the electrolyte performance, and the development of novel cathode materials. A Zn anode can be subjected to corrosion and dendrite formation. Dendrite formation and growth are associated with the uneven deposition of Zn, given by differences in electric field strength on the surface, gradients in ion concentration, and surface energy [13]. Uncontrolled dendrite growth can lead to dead Zn or separator piercing and cell failure. As briefly mentioned above, thermodynamically, HER inevitably occurs during Zn deposition, although its reaction rate is strongly mitigated under a mild acidic pH environment. HER can cause several issues like lower Coulombic efficiency (CE), electrolyte depletion, H_2 bubble formation with subsequent uneven metal deposition, and fluctuation in the pH value of the electrolyte, with possible corresponding byproduct formation [8]. The cathode side is also affected by a series of detrimental effects. The major issue, as reported for Mn-based, V-based, and Prussian Blue analogue-based cathodes, is the dissolution into the electrolyte during cycling with structural degradation, which worsens the electrochemical properties [14, 15]. Additionally, byproduct formation, usually Zn salts, can occur at the cathode surface, increasing interfacial charge transfer resistance and lowering cycle life. Different approaches have been proposed in the literature to solve or at least mitigate these problems, involving anode engineering [16], development and modifications of novel cathodes [17], and electrolyte optimisation [18].

Since parasitic reactions and dendrite growth occur at the electrode-electrolyte interface, the role played by the electrolyte is, without any doubt, fundamental. As Zn salts have a direct influence on various electrolyte properties such as pH value, ionic conductivity, working voltage window, and the reversibility of the Zn anode, several salts, including $ZnSO_4$, $ZnCl_2$, $Zn(ClO_4)_2$, $Zn(NO_3)_2$, $Zn(CH_3COO)_2$, $Zn(TFSI)_2$, and $Zn(CF_3SO_3)_2$, have been employed as electrolytes in ZIBs [19]. Electrolyte additives have been widely investigated to improve electrochemical performance and minimise degradation processes involving the electrolyte [20]. These include ionic species (e.g., Mn^{2+} [21], Al^{3+} [22]), organic compounds like citric acid or naphthalene [23], as well as metals and inorganic compounds, such as tin oxide [24] and phosphoric acid [25].

Besides liquid electrolytes, gel polymer electrolytes (GPE) have been demonstrated to substantially improve the anode reversibility, CE, and cycle life of the battery. Indeed, aqueous electrolytes inherently suffer from narrow electrochemical stability window and dendrite formation. The use of bio-polymer-based GPEs mitigates these challenges by reducing "free" water molecules activity and altering cation solvation, thereby enhancing stability and ionic transport. GPEs feature a 3D porous network composed of polymeric chains in which ions can move with more organised ion migration compared to liquid aqueous electrolytes. It promotes uniform ion flow and reduces the formation and growth of dendrites, also thanks to the mechanical resistance exerted in protrusions on the Zn anode [26, 27]. Functional groups along the polymeric chains play a pivotal role. Hydroxyl and carboxyl groups, for example, can interact with free H_2O with high electrochemical activity, converting it into bond water [28]. This phenomenon implies that a lower amount of free water will be available for HER, and the modification of the solvation structure of Zn^{2+} will also be reflected by lower overpotentials related to desolvation processes. Moreover, GPEs can

be coupled with advanced and well-engineered liquid electrolytes, combining the advantages of both liquid and polymer electrolytes. Many polymeric matrices based on poly(vinyl alcohol) - PVA [29, 30], poly(acrylamide) - PAM [31–33], poly(acrylic acid) - PAA [34], and other polymers have been reported in the literature [27]. In recent years, biopolymer-based GPEs have attracted significant attention. Compared to synthetic polymers, biopolymers offer clear advantages: they are environmentally sustainable, biodegradable, and rich in functional groups (e.g., −OH, −COOH) that facilitate ion transport and strengthen electrolyte–polymer interactions, which in turn lead to comparable or even improved electrochemical performance [35–37]. Traditional polymers, derived from nonrenewable resources, still provide better mechanical and thermal stability, which are important for applications such as wearable devices and highly demanding systems, but this advantage is less critical for large-scale storage, where cost, efficiency, and sustainability are primarily considered [31].

Furthermore, biopolymer-based gel electrolytes are characterised by low cost, low toxicity, and environmental friendliness, enabling their use in a wide range of applications, where biocompatibility is essential [38]. Among all the natural polymers, polypeptides and polysaccharides are the most commonly used to prepare bio-sourced GPEs, such as chitosan [39–42], agar [43–45], alginate [46–49], cellulose [6, 50], gelatin [51, 52], and xanthan gum [53, 54]. GPEs broaden the applicability of ZIBs to stationary energy storage, portable electronics, and flexible or wearable devices. Their quasi-solid structure enhances safety, prevents electrolyte leakage, and suppresses dendrite formation. At the same time, GPEs maintain mechanical integrity and contribute to improved cycling stability, making them attractive for both large-scale (seasonal/stationary) and miniaturised (wearables, smart-patches, etc.) energy storage systems [11].

Following an initial screening, agarose and alginate were identified as the most suitable candidates for a comparative study due to their rapid and straightforward preparation procedures, scalability potential, and capacity to form self-standing membranes, and are used in this study as polymeric hosts for 2M $ZnSO_4$ liquid electrolyte. Self-standing GPEs with high ionic conductivity and improved zinc deposition in Zn//Zn symmetric cells were obtained using facile and easy scalable preparation procedures [55, 56]. SEM and EDX analysis also confirmed these findings. The rate capability of GPEs was also evaluated in full cells using a novel CaV_6O_{16} $3H_2O$ cathode material never tested with bio-polymer-based GPE. Both bio-polymer-based GPEs delivered good specific discharge capacities, comparable with the results obtained from the liquid electrolyte or even better in terms of cyclability, as in the case of high-loading electrodes, which accounts for their promising prospects in developing novel, stable, and sustainable aqueous Zn-based batteries conceived for large-scale (seasonal) energy storage applications.

2 | Experimental Section

2.1 | Thermal Analysis

The thermogravimetric analysis (TGA) was conducted with a Netzsch TG-209-F3 instrument, in a temperature range between 25°C and 800°C under a nitrogen atmosphere (N_2 flux of 100 mL min^{-1}), using a heating ramp of 10°C min^{-1}.

2.2 | GPEs Preparation Procedures

All chemicals used in this study were purchased from Sigma-Aldrich. Agarose gel polymer electrolyte (AG-GPE) was obtained by adapting a preparation procedure reported in the literature [55]. A solution of agarose in water with a ratio of 1:15 in weight was prepared and stirred at 90°C until complete polymer dissolution, yielding a clear and homogeneous solution. The solution was then cast using a doctor blade, allowing for better control of the thickness to 1 mm, and soaked in 2M $ZnSO_4$.

Sodium alginate gel polymer electrolyte (SA-GPE) was also obtained by adapting a preparation procedure reported in the literature [56]. A solution of sodium alginate and water with a ratio of 1:20 in weight was prepared to facilitate homogeneous mixing using a thinky mixer. Once the homogeneous solution was obtained, it was cast using the doctor blade to obtain a 1 mm thickness. The cast solution was then directly wet with 2M $ZnSO_4$ to allow Zn^{2+} ionic crosslinking. As the final step, the obtained SA-GPE was soaked in 2M $ZnSO_4$. The thickness of both AG- and SA-GPEs ranged between 500 and 700 μM.

2.3 | Investigation of Zn Electrode Morphologies After Cycling

Scanning electron microscopy (SEM) images were collected with 5 keV electrons using an in-lens detector of a Zeiss SUPRA 40 (Zeiss SMT, Oberkochen, Germany) field emission electron microscope (FESEM). Evaluation of Zn electrode morphologies with SEM was performed after plating and stripping in Zn//Zn symmetric cells cycled at 2 mA cm^{-2} with 2 mAh cm^{-2} plated/stripped capacity per half-cycle for 100 cycles. The recovered Zn electrodes were washed three times with ethanol before characterisation.

2.4 | Electrochemical Characterisation of GPEs

Electrochemical behaviour of GPEs and 2M $ZnSO_4$ was evaluated by housing the materials in two-electrode electrochemical test cells (ECC-Std by EL-Cell, Germany). Zn metal foils were cut into 10 mm diameter discs, and Whatman GF-A was used as the separator for 2M $ZnSO_4$ liquid electrolyte, while for AG-GPE and SA-GPE, no separators or spacers were used. Ionic conductivity was evaluated by electrochemical impedance spectroscopy (EIS) of symmetric SS//SS (stainless steel) cells within a frequency range of 500 kHz–100 mHz and applying a sinusoidal voltage signal (DV) of 20 mV. The values of ionic conductivity (σ) were calculated using the $\sigma = l/(RA)$ equation, where l represents the thickness, A the contact area of the electrolyte, and R the bulk resistance obtained from EIS measurement. The electrochemical stability window (ESW) was evaluated using linear sweep voltammetry (LSV) of Zn//SS cells in the potential range of 0–3 V versus Zn^{2+}/Zn at 0.1 mV s^{-1}. Cyclic voltammetry (CV) tests were performed in Zn//Ni cells between −0.3 and 1 V versus Zn^{2+}/Zn with a sweep rate of 0.2 mV s^{-1}. Reversible plating and stripping

capability was tested in Zn//Zn symmetric cells by galvanostatic cycling at various current densities of 0.25, 0.5, 1, and 2 mA cm^{-2} with a total exchanged capacity per half-cycle of 0.25 mAh cm^{-2}. After the various current density steps, long-term cycling capability was evaluated at 0.5 mA cm^{-2}. For the evaluation of Zn electrode morphologies by SEM analysis, electrodes were cycled at 2 mA cm^{-2} with 2 mAh cm^{-2} capacity for 100 cycles.

2.5 | Electrochemical Characterisation of Zn || $CaV_6O_{16}{\cdot}3H_2O$ Full Cells

Electrochemical characterisation of full ZIB cells was performed in ECC-Std two-electrode cells. The CaV_6O_{16} $3H_2O$ cathode material was synthesised as reported in a previous work [57]. The cathode slurry was prepared by mixing the active material $CaV_6O_{16}{\cdot}3H_2O$, the electronically conducting additive (Timcal C-65 carbon black powder), and the polymeric binder poly (vinylidene fluoride) - PVDF (Solvay Solef) with a weight ratio of 7:2:1 in N-methyl-2-pyrrolidone (NMP) solvent. The slurry was cast on a carbon gas diffusion layer (GDL, AvCarb EP40T) and cut into 10 mm diameter discs. The electrodes (active mass loading of approximately 2.5 and 5 mg cm^{-2}) were then dried in a Buchi oven overnight at 70°C and then transferred to the glove-box for further cell assembly. Ambient temperature galvanostatic charge-discharge measurements of the laboratory-scale ZIBs were performed at different current densities (from 50 to 2000 mA g^{-1}) in the 0.2 to 1.6 V versus Zn^{2+}/Zn voltage range.

3 | Results and Discussion

3.1 | Electrochemical Characterisation of Gel Polymer Electrolytes

Both AG-GPE and SA-GPE were prepared with fast and facile preparation procedures as briefly illustrated in Figure 1 [55, 56]. The gelation of the two biopolymers occurs through different mechanisms.

In AG-GPE, gelation occurs during the cooling process. After casting, agarose forms single or double helix structures through physical crosslinking that bonds one with another, contributing to the formation of the 3D network of the gel electrolyte. Sodium alginate chains instead consist of mannuronic acid (M) and guluronic acid (G) units, organised in segments rich in G units, segments rich in M units, and segments in which G and M units alternate [46, 47]. Divalent cations, such as Zn^{2+}, play the crucial role of ionic crosslinkers between the carboxylate groups at the guluronic acid units, promoting the formation of a highly interconnected polymeric framework of the gel polymer electrolyte. Thermogravimetric analysis (TGA) revealed that both materials exhibited a similar behaviour, characterised by the initial evaporation of the water-based electrolyte starting at ambient conditions (retaining ca. 45% of their initial mass, as shown in Supporting Information S1: Figure S5a) and completing upon heating at approximately 100°C (Supporting Information S1: Figure S5b). Overall, both samples turned out to be composed of ca. 70% of water and 30% of solid content (including polymer matrixes and electrolyte salts). Both AG-GPE and SA-GPE also displayed a

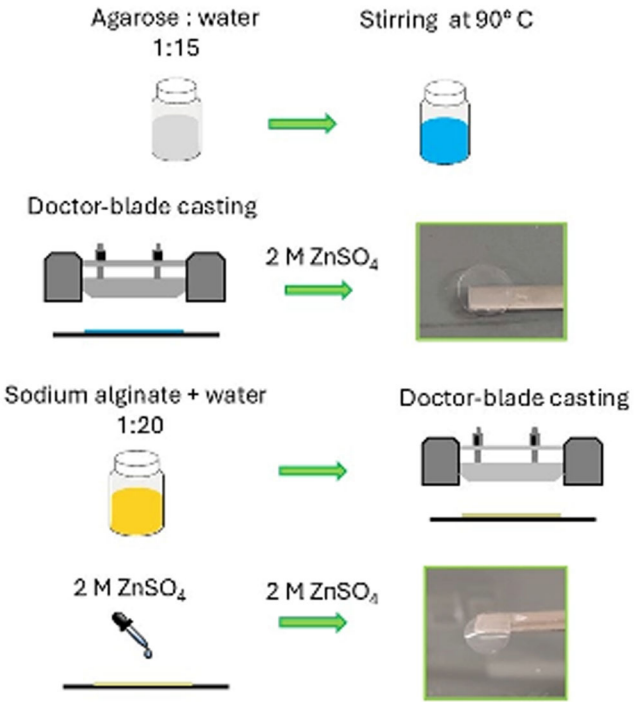

FIGURE 1 | Schematic illustration of the simple preparation procedures for agarose-based GPE, AG-GPE (a), and sodium alginate-based GPE, SA-GPE (b).

TABLE 1 | Comparison of ionic conductivity, Coulombic efficiency (CE) of Zn metal, and electrochemical stability window (ESW) for the electrolytes under study.

	2 M $ZnSO_4$	SA-GPE	AG-GPE
Ionic conductivity	3.5×10^{-2} S cm^{-1}	2.5×10^{-2} S cm^{-1}	3.9×10^{-2} S cm^{-1}
CE	30%	55%	76%
ESW	1.7 V	1.9 V	2 V

major degradation event of the polymer matrix occurring at about 300°C [58, 59]. Based on the obtained results, the polymer content in the GPEs was estimated to be approximately 7%, while the remaining fraction consisted of inorganic salt electrolyte. Generally, these findings indicate that both formulations possess comparable electrolyte-holding properties.

Ionic conductivity of GPEs was evaluated by EIS at room temperature. Table 1 reports the conductivity values of the prepared GPEs and the 2 M $ZnSO_4$ solution. Indeed, the 2 M $ZnSO_4$ showed an ionic conductivity of 3.5×10^{-2} S cm^{-1}, SA-GPE of 2.5×10^{-2} S cm^{-1}, while AG-GPE achieved the highest value of 3.9×10^{-2} S cm^{-1} among the electrolytes under study. The excellent ionic conductivities of SA-GPE and AG-GPE, comparable to the results obtained with the 2 M $ZnSO_4$, indicate that ion movement is unaffected or hindered by the polymeric network. The obtained conductivity values are in line with those reported for similar systems in the literature [43, 47, 55, 56] and are suitable for applications in electrochemical storage systems

operating at high current densities at ambient conditions. Although the measured conductivities are high, even higher values can be obtained in aqueous systems. It should be emphasised that the polymer matrix in GPE formulations generally affects ionic conductivity by hindering the mobility of ionic species. Reducing the polymer content represents a straightforward strategy to mitigate this drawback; however, such an approach may compromise the mechanical integrity of the material. Moreover, in aqueous systems, the most mobile ionic species are H_3O^+ and OH^-. At pH 5.5, their concentration is relatively low, thus in turn their contribution to the overall ionic mobility is limited. Furthermore, ionic conductivity values obtained are comparable to those reported for GPE based on other polymers. For example, chitosan- and cellulose-based electrolytes demonstrated ionic conductivities of about 25 and 26 mS cm^{-1}, respectively [60, 61]. Similar trends were also observed for non-biosourced GPEs, such as PVA/PAM systems, which exhibited ionic conductivity in the order of 14 mS cm^{-1} [61].

Linear sweep voltammetry (LSV) was used to evaluate the electrochemical stability window (ESW) of the two GPEs and the 2 M $ZnSO_4$ electrolyte. Figure 2a shows the current response of the Zn//SS cells employing the 2 M $ZnSO_4$ (blue line), SA-GPE (yellow line), and AG-GPE (green line) electrolytes, evidencing ESWs of 1.7, 1.9, and 2 V, respectively, defined by considering a limit leakage current, associated with the OER process, of 10 μA cm^{-2}. Results show an extended ESW of the prepared GPEs compared to the liquid electrolyte, indicating

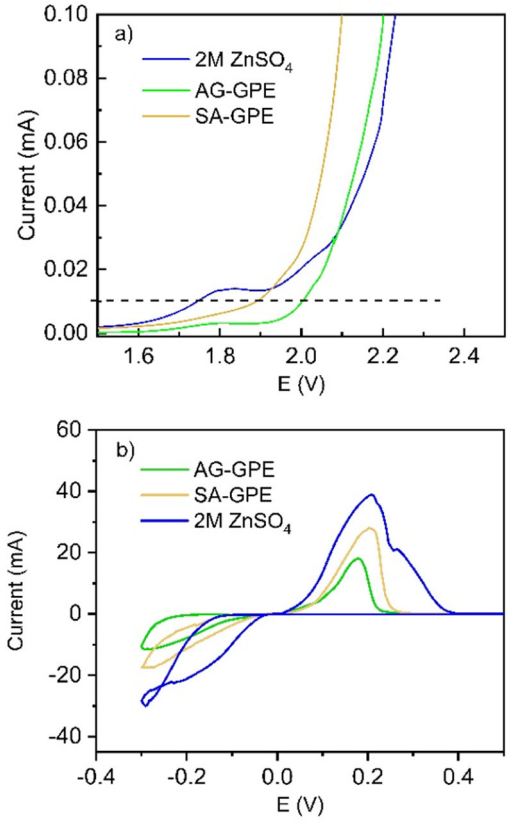

FIGURE 2 | (a) Linear sweep voltammetry in Zn//SS cells of 2 M $ZnSO_4$ (blue), SA-GPE (yellow) and AG-GPE (green). (b) Cyclic voltammetry (CV) in Zn//Ni cells for 2 M $ZnSO_4$ (blue), SA-GPE (yellow) and AG-GPE (green).

enhanced stability against oxidative (anodic) potentials, most likely associated with the reduced availability of free water for the OER process [62]. The cyclic voltammetry of the Zn//Ni cells (Figure 2b) shows the characteristic behaviour of metal deposition processes. The measurement evidence a higher peak current for the liquid electrolyte. However, by calculating the CE by integrating the area of the peak current, the 2 M liquid $ZnSO_4$ electrolyte had the lowest efficiency (30%), while both the SA-GPE and AG-GPE showed improved efficiencies of 55% and 76%, respectively.

Metal anode-electrolyte compatibility and stability are key parameters in an electrochemical cell, particularly in aqueous batteries. In aqueous media, Zn electrodes can be affected by several detrimental effects like corrosion, passivation, dendrite formation, and HER; all phenomena in which the pH of the electrolyte also plays a crucial role [8, 63]. Thus, the electrolytes under study were tested for their reversible plating and stripping behaviour in Zn//Zn symmetrical cells to evaluate Zn deposition and stripping stability and reversibility. The results obtained for 2 M $ZnSO_4$, SA-GPE, and AG-GPE are shown in Figure 3a–c, while the direct comparison of the three systems upon long-term cycling is shown in Figure 3d.

The 2 M $ZnSO_4$ liquid electrolyte-based cell showed a stable plating and stripping behaviour up to 1 mA cm^{-2} with a voltage polarisation of about 100 mV at 0.25 mA cm^{-2}. However, during cycling at 2 mA cm^{-2}, a drop in voltage polarisation can be clearly noted, most likely due to uneven Zn stripping and deposition and dendrite formation, as also evidenced in the SEM images shown in Figure 4c,d. Non-homogeneous deposition and dendrite formation are well documented in the literature for liquid electrolytes [39, 61]. Several factors, such as ion concentration gradients, surface energy, and electric field strength, influence the nucleation of Zn. An example is the "tip effect", whereby a localised higher electric field promotes preferential deposition of Zn cations in some regions at the Zn electrode surface. As the deposition process continues, the area close to the tip becomes depleted of Zn cations, leading to a variation of Zn^{2+} concentration on the surface of the electrode that further exacerbates dendrite growth. It is worth mentioning that dendrites can lead to dead Zn or short-circuiting of the cell due to separator piercing. Additionally, they provide more sites where HER, corrosion, and passivation could occur. On the contrary, by using the prepared GPEs, it is evident that there is a more stable plating and stripping behaviour with respect to the 2 M $ZnSO_4$ liquid electrolyte. Moreover, the test carried out using the GPEs shows a lower voltage polarisation at all of the tested current densities. Amongst the two developed GPEs, AG-GPE showed an almost ideal voltage profile and the lowest voltage polarisation values of 20, 50, 85, and 115 mV at 0.25, 0.5, 1, and 2 mA cm^{-2}, respectively, while the liquid electrolyte showed voltage polarisations of 110, 115, 130, and 150 mV at the same current densities. In Figure 4d, the comparison between 2 M $ZnSO_4$, SA-GPE, and AG-GPE upon long-term cycling at 0.5 mA cm^{-2} is shown. Both GPEs outperformed the liquid electrolyte-based cell in terms of long-term performance. SA-GPE maintained the stripping and deposition for around 425 h; however, it evidences a sudden increase in polarisation, most likely associated with uneven deposition of the Zn, leading to cell failure due to short circuit related to dendrite formation.

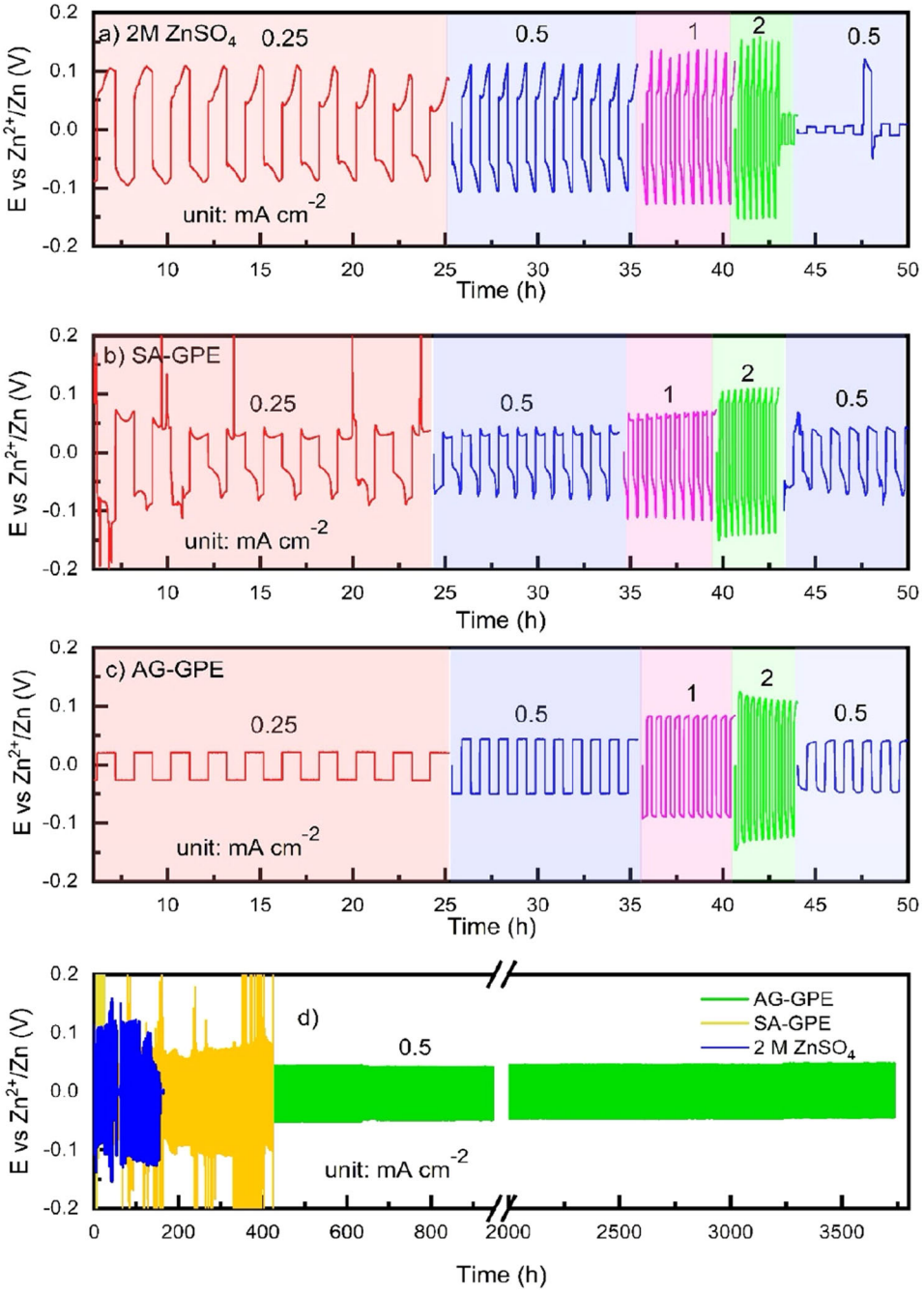

FIGURE 3 | Rate capability test of Zn//Zn cells at various current densities from 0.25 to 2 mA cm^{-2}, plated/stripped capacity per half-cycle of 0.25 mAh cm^{-2}: (a) 2 M $ZnSO_4$, (b) SA-GPE, (c) AG-GPE. (d) Long-term Zn plating-stripping voltage profiles at 0.5 mA cm^{-2}, with 0.25 mAh cm^{-2}.

Instead, AG-GPE showed superior cycling stability, maintaining a low and almost constant polarisation for more than 3800 h, with a very stable voltage profile suggesting a smooth and homogeneous deposition of Zn.

The enhanced performances of AG-GPE are ascribed to its ability to mitigate parasitic reactions and promote an efficient and stable Zn-metal deposition and stripping, driven by the synergistic effects of two contributions related to the polymer matrix and its hydroxyl-rich functional groups. The first one is the guiding effect of polymeric chains and their functional groups on the diffusion of Zn cations. Carboxylate groups of sodium alginate restrain Zn cations' movement, hindering their diffusion in regions of the electrodes where the "tip effect" occurs, implying the slowing and mitigation of dendrite growth [56]. The second one is the capability of GPEs to perturb and alter the solvation structure of Zn^{2+}, thanks to the presence of −OH groups along the polymeric chains. The interaction of −OH groups through hydrogen bonds with water severely limits the mobility and hydration effect of Zn^{2+}, contributing to stable electrodeposition [55]. In addition, −OH groups can also limit the free diffusion of SO_4^{2-}, lowering the formation of byproducts.

SEM imaging of Zn electrodes after 100 cycles of plating and stripping at 2 mA cm^{-2} with a capacity of 2 mAh cm^{-2} (see

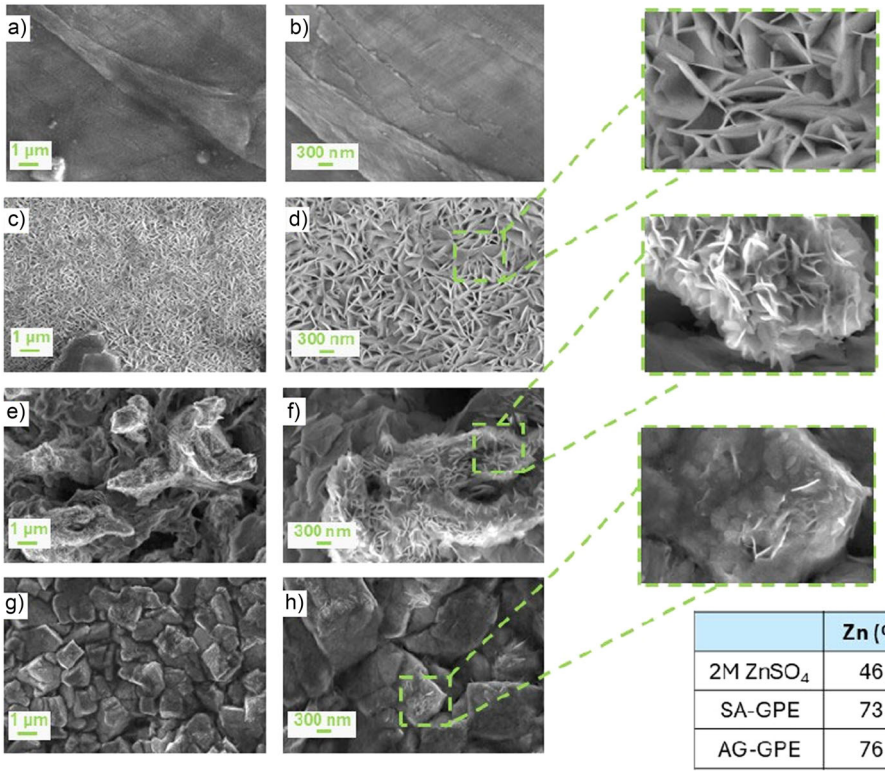

	Zn (%wt)	C (%wt)	O (%wt)	S (%wt)
2M $ZnSO_4$	46.63	//	37.54	15.83
SA-GPE	73.98	6.76	17.27	2
AG-GPE	76.63	13.71	9.12	0.55

FIGURE 4 | SEM images with corresponding EDX analysis of Zn foils morphologies after 100 cycles at 2 mA cm^{-2} with plated/stripped capacity per half-cycle of 2 mAh cm^{-2}. (a, b) Pristine zinc, (c, d) 2 M $ZnSO_4$, (e, f) SA-GPE, (g, h) AG-GPE.

Figure S1 in the Supporting Information) was performed to evaluate the influence of the electrolyte composition on the Zn deposition morphology. Figure 4 shows SEM images of the Zn electrode in pristine condition (Figure 4a,b), and after cycling in 2 M $ZnSO_4$ (Figure 4c,d), SA-GPE (Figure 4e,f) and AG-GPE (Figure 4g,h), while the table reports results obtained from EDX analysis (corresponding images with EDX maps are shown in the Supporting Information: Figures S2, S3, and S4).

As expected from the electrochemical results, the Zn metal recovered by the cell using the 2 M $ZnSO_4$ electrolyte exhibited an uneven deposition morphology, with a widespread presence of flake-like dendrites at all the magnifications (Figure 4c,d). On the contrary, SA-GPE (Figure 4e,f) and AG-GPE (Figure 4g,h) resulted in a relatively uniform surface deposition of the Zn after cycling. In particular, the Zn electrodes recovered from the cell using SA-GPE exhibited tree-like structures uniformly distributed on the surface, along with flakes that have smaller dimensions than those found in the liquid electrolyte. The Zn electrodes recovered from the cell using AG-GPE showed a uniform formation of plates and plate-like structures with negligible amounts of flake-like dendrites. It agrees with the plating-stripping results (Figure 3), which account for enhanced ability to promote even Zn deposition, preventing the formation of dendrites. As clearly shown by plating and stripping results and SEM analysis, the introduction of a GPE has a significant impact on the anode-electrolyte interface. The polymeric matrix and its functional groups have a beneficial effect on zinc deposition, improving homogeneity. Through hydrogen bonding with water molecules, these groups modify the cation solvation shell, lowering desolvation energies and suppressing HER. In contrast, liquid electrolytes lack this confinement, leading to more free water at the electrode interface, enhanced HER, dendrite growth, and higher by-product formation due to the reactivity of uncoordinated anions and water molecules [64, 65]. Moreover, the different surface morphologies observed for the GPEs suggest that the polymeric matrix also plays a role in the deposition of Zn metal and, as a consequence, in the resulting morphology of Zn electrodes. EDX measurements were carried out to evaluate the elemental composition at the Zn electrode surface. Figure 4 shows the elemental composition, revealing a notable difference in oxygen and sulphur content. The presence of these elements on the electrode surface arises from the formation of byproducts like Zn hydroxysulfate ($Zn_4(OH)_6SO_4{\cdot}5H_2O$) [46]. $Zn_4(OH)_6SO_4{\cdot}5H_2O$ formed at the Zn electrode surface, where water from the solvation sheaths of Zn^{2+} and diffused SO_4^{2-} participate in parasitic redox reactions [66–68]. These reactions and their byproducts contribute to dendrite formation and Zn consumption. Compared to the liquid electrolyte, both GPEs present a lower amount of oxygen (O %wt: 17.27 and 9.12 for SA-GPE and AG-GPE, respectively) and sulphur (S %wt: 2 and 0.55 for SA-GPE and AG-GPE, respectively). It suggests that GPEs can reduce the formation of byproducts, substantially improving the cyclability of Zn anodes, and particularly agarose in AG-GPE, having the lowest amounts of O and S, can substantially mitigate side reactions at the surface of the Zn anode electrode. These findings are also confirmed by XRD analysis of Zn anodes after cycling for similar GPEs reported in literature [5, 31, 69]. Both SEM and EDX analyses provide insight into the fading mechanism highlighted in the plating and stripping results. The ex-situ analysis clearly shows an improved deposition morphology, with limited formation of byproducts and dendrites in GPE-based

cells, thanks to the previously described effects on the deposition of the polymeric backbone and functional groups of the electrolytes. Additionally, SEM and EDX analyses can provide insight into the reduced plating/stripping stability of SA-GPE. SEM shows the presence of fine, flake-like dendrites on the SA-GPE surface, which can expand during cycling and induce short-circuiting. EDX further detects higher oxygen and sulphur contents, indicating the formation of by-products that passivate the Zn surface, promote uneven deposition, and reduce cycling stability.

The electrochemical behaviour of the prepared SA-GPE and AG-GPE was confirmed in laboratory-scale Zn-ion cells, using Ca-$V_6O_{16}{\cdot}3H_2O$ (CVO) cathode material, and compared with 2 M $ZnSO_4$ liquid electrolyte. Notably, to our knowledge, CVO was never tested before with these biopolymer-based GPEs in Zn-based cells [57]. Zn//CVO electrochemical cells were assembled with two different active material loadings of 2.5 mg cm^{-2} (low) and 5 mg cm^{-2} (high). The galvanostatic cycling tests were performed using different specific currents ranging from 50 to 2000 mA g^{-1}; after the rate capability test at various current densities, the cells were cycled

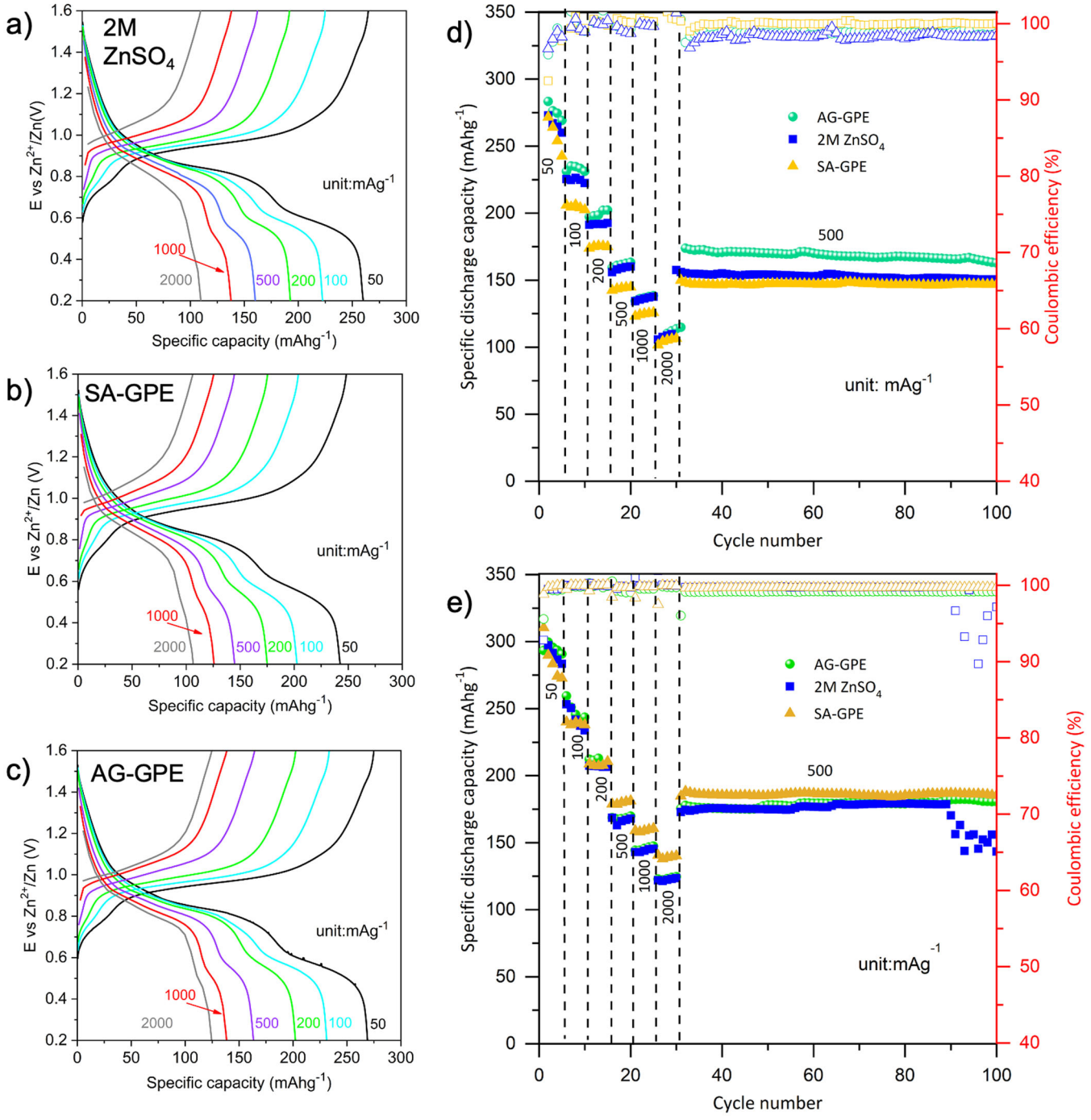

FIGURE 5 | Galvanostatic charge-discharge voltage versus specific capacity profiles for Zn//CVO full cells with different electrolytes: (a) 2 M $ZnSO_4$ liquid electrolyte, and (b) SA-GPE, (c) AG-GPE; and rate capability galvanostatic tests at various current densities for (d) 2.5 mg cm^{-2} cathode loading, and (e) 5 mg cm^{-2} cathode loading.

to 100 cycles at a fixed 500 mA g^{-1} current. Figure 5a–c show the galvanostatic charge-discharge voltage versus specific capacity profiles for 2 mg cm^{-2} cathode loading for 2 M $ZnSO_4$, SA-GPE, and AG-GPE, respectively. Figure 5d shows the rate capability for the low loading cell (2.5 mg cm^{-2} active material loading), while Figure 5e shows the same test for the high loading cell (5 mg cm^{-2}). Representative voltage profiles recorded from the cycling test performed with the low loading electrode, Figure 5a–c, evidencing two different plateaus, indicate that intercalation of Zn^{2+} in CVO cathode occurs through a multistep process; moreover, H^+ co-insertion in vanadium-based cathodes was also already reported [57, 70]. The capacity and storage mechanism of vanadium-based cathodes is controlled by both capacitive and diffusive processes [71]. Reversibility, structural stability, and high capacities of these materials depend on crystalline polymorphs, particle size, and components [72]. Common V_2O_5 is subjected to structural degradation upon repeated intercalation and de-intercalation of Zn^{2+}. In recent years, the insertion of alkali and transition metals in the cathode structure has emerged as a possible solution. Metals like Na [73, 74], Li [75], Zn [76–78] and Ca [79, 80] act as pillaring agents in the layered structure of the cathode significantly improving structural stability.

Specifically, Ca contributes to increased interlayer spacing, promoting easy and efficient insertion of Zn^{2+} [54, 81]. Additionally, structural H_2O has been shown to enhance and improve the electrochemical performance of V-based cathodic materials. H_2O molecules intercalated within the layered structure also play a crucial role in widening interlayer distances and improving structural flexibility. Moreover, the electrostatic shielding effect of Zn^{2+} interactions with the cathodic host material guarantee a facile Zn^{2+} diffusion [82–84].

Figure 5d,e show the rate capability tests of the electrolytes assembled in cells with two different active material loadings. At low 2.5 mg cm^{-2} loading (Figure 5d), both SA-GPE and AG-GPE delivered good specific discharge capacities, similar to the capacities delivered by the liquid electrolyte. In the first cycle, 2 M $ZnSO_4$, SA-GPE, and AG-GPE delivered 273, 271, and 283 mAh g^{-1} with coulombic efficiencies of 97%, 92%, and 95%, respectively, that gradually increased upon cycling, demonstrating overall good reversibility.

The irreversible capacity in the first cycles likely derives from the parasitic reaction of O_2 reduction [85]. Although the de-aeration of 2 M $ZnSO_4$ was conducted by N_2 bubbling, all cells were assembled in an open-air environment, leading to some unavoidable presence of dissolved oxygen. In particular, SA-GPE delivered slightly lower specific capacities than 2 M $ZnSO_4$ at 100, 200, 500, and 1000 mA g^{-1}, while similar rate capabilities were obtained at 2000 mA g^{-1}, as well as upon the more prolonged cycling at 500 mA g^{-1}. AG-GPE showed rate capabilities almost identical to that of the liquid electrolyte at the various current densities, while during the prolonged cycling at 500 mA g^{-1}, AG-GPE delivered about 20 mAh g^{-1} more than $ZnSO_4$.

At high 5 mg cm^{-2} cathode loading (Figure 5e), the initial irreversible capacity remains evident and is attributed to the parasitic reactions previously described. As the cathode loading increases, the amount of Zn participating in plating and stripping at the anode also rises, due to the greater capacity of the cathode to accommodate Zn ions. Testing rate capabilities under high-loading conditions is particularly important, as it better represents practical operating conditions and helps at avoiding overestimations of performance that may arise from low-loading configurations. In such cases, limited Zn utilisation at the anode and reduced electrochemical and mechanical stresses at the electrode/electrolyte interfaces can mask degradation phenomena. Conversely, higher loadings amplify these effects, accelerating failure mechanisms and enabling their earlier detection.

Even under these demanding conditions, the gel polymer electrolytes (GPEs) exhibited superior rate capability and consistently high coulombic efficiency across all tested current densities, outperforming the liquid electrolyte. Notably, the cell containing 2 M $ZnSO_4$ electrolyte failed after the 90th cycle, whereas both AG-GPE and SA-GPE sustained operation until the end of the experiment. These results demonstrate that the use of GPEs significantly enhances the stability of the charge–discharge processes, thereby improving both the efficiency and the cycling life of the cells.

4 | Conclusions

In this work, a comparative study is presented of two bio-sourced gel polymer electrolytes (GPEs) to be used in the next generation of green, sustainable aqueous Zn-based batteries (ZIB). They were prepared via simple and rapid procedures and demonstrated ability to enhance electrochemical performance in both symmetric and full cells employing a novel CaV_6O_{16}-based cathode material not previously tested with GPEs in laboratory-scale ZIB. The SA-GPE and AG-GPE exhibited high ionic conductivities of 2.5×10^{-2} and 3.9×10^{-2} S cm^{-1}, respectively, which are comparable to those of conventional liquid electrolytes. Owing to the synergistic effects of the polymer chains guiding Zn^{2+} diffusion and the presence of abundant hydroxyl groups that modify Zn^{2+} solvation structures, both electrolytes enabled stable Zn plating/stripping at high current densities (0.5 mA cm^{-2}), maintaining remarkably stable performance for 400 h with SA-GPE and over 3500 h with AG-GPE. The enhanced electrode–electrolyte interfacial stability was further confirmed by SEM and EDX analyses, which revealed suppressed dendrite formation and reduced by-product accumulation.

Interestingly, the surface morphology of Zn electrodes differed depending on whether alginate- or agarose-based GPEs were used, indicating a strong influence of the polymer matrix on the Zn deposition mechanism. In full cell configurations with CVO cathodes, both GPEs delivered specific capacities and Coulombic efficiencies comparable to those achieved with 2M $ZnSO_4$ at low cathode loadings. Remarkably, under higher loading conditions, the $ZnSO_4$-based cell failed prematurely, highlighting the superior stability, efficiency, and cycle life imparted by the GPEs, consistent with the results observed in symmetric cells, and demonstrating the promising prospects of the newly developed materials for their practical application in next-generation, sustainable, and high-performing Zn-based batteries conceived for large-scale (seasonal) energy storage.

Acknowledgements

The HIPERZAB project (https://hiperzab.eu/en) has received funding from the European Union's EIC research and innovation programme under grant agreement No 101115421. Views and opinions expressed are, however, those of the author(s) only and do not necessarily reflect those of the European Union. Neither the European Union nor the granting authority can be held responsible for them. Part of this study was carried out within the activities "Ricerca Sistema Elettrico" 2025-27 funded through contributions to research and development by the Italian Ministry of Economic Development. Support under the MUR program "Dipartimenti di Eccellenza 2023–2027" (CUPE17G22001490006) is gratefully acknowledged. Open access publishing facilitated by Politecnico di Torino, as part of the Wiley - CRUI-CARE agreement.

Conflicts of Interest

The authors declare no conflicts of interest.

Data Availability Statement

Data available on request from the authors.

References

1. M. Li, J. Lu, Z. Chen, and K. Amine, "30 Years of Lithium-Ion Batteries," *Advanced Materials* 30, no. 33 (2018): 1800561.

2. B. E. Lebrouhi, S. Baghi, B. Lamrani, E. Schall, and T. Kousksou, "Critical Materials for Electrical Energy Storage: Li-Ion Batteries," *Journal of Energy Storage* 55 (2022): 105471.

3. S. Dühnen, J. Betz, M. Kolek, R. Schmuch, M. Winter, and T. Placke, "Toward Green Battery Cells: Perspective on Materials and Technologies," *Small Methods* 4, no. 7 (2020): 2000039.

4. C. Delmas, "Sodium and Sodium-Ion Batteries: 50 Years of Research," *Advanced Energy Materials* 8, no. 17 (2018): 1703137.

5. H. Wang, A. Zhou, Z. Hu, et al., "Toward Simultaneous Dense Zinc Deposition and Broken Side-Reaction Loops in the $Zn//V_2O_5$ System," *Angewandte Chemie* 136, no. 11 (2024): e202318928.

6. D. Wang, H. Li, Z. Liu, et al., "A Nanofibrillated Cellulose/Polyacrylamide Electrolyte-Based Flexible and Sewable High-Performance $Zn–MnO_2$ Battery With Superior Shear Resistance," *Small* 14, no. 51 (2018): 1803978.

7. W. Manalastas, Jr., S. Kumar, V. Verma, L. Zhang, D. Yuan, and M. Srinivasan, "Water in Rechargeable Multivalent-Ion Batteries: An Electrochemical Pandora's Box," *Chemsuschem* 12, no. 2 (2019): 379–396.

8. M. Liu, P. Wang, W. Zhang, et al., "Strategies for pH Regulation in Aqueous Zinc Ion Batteries," *Energy Storage Materials* 67 (2024): 103248.

9. D. Frattini, E. G. Gaitán, A. B. Murguialday, M. Armand, and N. Ortiz -Vitoriano, "Essential Data for Industrially Relevant Development of Bifunctional Cathodes and Biopolymer Electrolytes in Solid-State Zinc–Air Secondary Batteries," *Energy & Environmental Science* 15, no. 12 (2022): 5039–5058.

10. E. García-Gaitán, M. C. Morant-Miñana, D. Frattini, et al., "Agarose-Based Gel Electrolytes for Sustainable Primary and Secondary Zinc-Air Batteries," *Chemical Engineering Journal* 472 (2023): 144870.

11. J. Zhu, Z. Tie, S. Bi, and Z. Niu, "Towards More Sustainable Aqueous Zinc-Ion Batteries," *Angewandte Chemie* 136, no. 22 (2024): e202403712.

12. G. Nazir, A. Rehman, J.-H. Lee, et al., "A Review of Rechargeable Zinc–Air Batteries: Recent Progress and Future Perspectives," *Nano-Micro Letters* 16, no. 1 (2024): 138.

13. C. Li, X. Xie, S. Liang, and J. Zhou, "Issues and Future Perspective on Zinc Metal Anode for Rechargeable Aqueous Zinc-Ion Batteries," *Energy & Environmental Materials* 3, no. 2 (2020): 146–159.

14. F. Wan and Z. Niu, "Design Strategies for Vanadium-Based Aqueous Zinc-Ion Batteries," *Angewandte Chemie International Edition* 58, no. 46 (2019): 16358–16367.

15. G. Li, L. Sun, S. Zhang, et al., "Developing Cathode Materials for Aqueous Zinc Ion Batteries: Challenges and Practical Prospects," *Advanced Functional Materials* 34, no. 5 (2024): 2301291.

16. Q. Wen, H. Fu, R. Cui, et al., "Recent Advances in Interfacial Modification of Zinc Anode for Aqueous Rechargeable Zinc Ion Batteries," *Journal of Energy Chemistry* 83 (2023): 287–303.

17. A. Kim, Y. Park, J. Choi, S.-H. Yu, and K. W. Nam, "A Comprehensive Review of Cathode Materials for Advanced Aqueous Zinc-Ion Batteries," *ACS Applied Energy Materials* 8 (2025): 6806–6828.

18. J. Wei, P. Zhang, J. Sun, et al., "Advanced Electrolytes for High-Performance Aqueous Zinc-Ion Batteries," *Chemical Society Reviews* 53 (2024): 10335–10369.

19. Y. Wang, Z. Wang, F. Yang, et al., "Electrolyte Engineering Enables High Performance Zinc-Ion Batteries," *Small* 18, no. 43 (2022): 2107033.

20. S. Guo, L. Qin, T. Zhang, et al., "Fundamentals and Perspectives of Electrolyte Additives for Aqueous Zinc-Ion Batteries," *Energy Storage Materials* 34 (2021): 545–562.

21. D. Chao, W. Zhou, C. Ye, et al., "An Electrolytic $Zn–MnO_2$ Battery for High-Voltage and Scalable Energy Storage," *Angewandte Chemie* 131, no. 23 (2019): 7905–7910.

22. T. M. C. Faro, G. P. Thim, and M. S. Skaf, "A Lennard-Jones Plus Coulomb Potential for Al^{3+} Ions in Aqueous Solutions," *Journal of Chemical Physics* 132, no. 11 (2010): 114509.

23. R. K. Ghavami and Z. Rafiei, "Performance Improvements of Alkaline Batteries by Studying the Effects of Different Kinds of Surfactant and Different Derivatives of Benzene on the Electrochemical Properties of Electrolytic Zinc," *Journal of Power Sources* 162, no. 2 (2006): 893–899.

24. H.-I. Kim and H.-C. Shin, "SnO Additive for Dendritic Growth Suppression of Electrolytic Zinc," *Journal of Alloys and Compounds* 645 (2015): 7–10.

25. C. W. Lee, K. Sathiyanarayanan, S. W. Eom, H. S. Kim, and M. S. Yun, "Novel Electrochemical Behavior of Zinc Anodes in Zinc/Air Batteries in the Presence of Additives," *Journal of Power Sources* 159, no. 2 (2006): 1474–1477.

26. M. Li, Z. Li, X. Wang, et al., "Comprehensive Understanding of the Roles of Water Molecules in Aqueous Zn-Ion Batteries: From Electrolytes to Electrode Materials," *Energy & Environmental Science* 14, no. 7 (2021): 3796–3839.

27. K. Wu, J. Huang, J. Yi, et al., "Recent Advances in Polymer Electrolytes for Zinc Ion Batteries: Mechanisms, Properties, and Perspectives," *Advanced Energy Materials* 10, no. 12 (2020): 1903977.

28. R. Qi, W. Tang, Y. Shi, et al., "Gel Polymer Electrolyte Toward Large-Scale Application of Aqueous Zinc Batteries," *Advanced Functional Materials* 33, no. 47 (2023): 2306052.

29. S. Huang, F. Wan, S. Bi, J. Zhu, Z. Niu, and J. Chen, "A Self-Healing Integrated All-in-One Zinc-Ion Battery," *Angewandte Chemie International Edition* 58, no. 13 (2019): 4313–4317.

30. W. Zhou, J. Chen, M. Chen, et al., "An Environmentally Adaptive Quasi-Solid-State Zinc-Ion Battery Based on Magnesium Vanadate Hydrate With Commercial-Level Mass Loading and Anti-Freezing Gel Electrolyte," *Journal of Materials Chemistry A* 8, no. 17 (2020): 8397–8409.

31. J. Cong, X. Shen, Z. Wen, et al., "Ultra-Stable and Highly Reversible Aqueous Zinc Metal Anodes With High Preferred Orientation

Deposition Achieved by a Polyanionic Hydrogel Electrolyte," *Energy Storage Materials* 35 (2021): 586–594.

32. Z. Shen, Y. Liu, Z. Li, et al., "Highly-Entangled Hydrogel Electrolyte for Fast Charging/Discharging Properties in Aqueous Zinc Ion Batteries," *Advanced Functional Materials* 35 (2024): 2406620.

33. T.-T. Li, P. Chen, X. Fu, et al., "Enhanced Stability-Based Hydroxymethyl Cellulose/Polyacrylamide Interpenetrating Dual Network Hydrogel Electrolyte for Flexible Yarn Zinc-Ion Batteries," *Journal of the Electrochemical Society* 171 (2024): 070511.

34. W. Lao-atiman, T. Julaphatachote, P. Boonmongkolras, and S. Kheawhom, "Printed Transparent Thin Film Zn-MnO_2 Battery," *Journal of the Electrochemical Society* 164, no. 4 (2017): A859–A863.

35. F. Wang, J. Zhang, H. Lu, et al., "Production of Gas-Releasing Electrolyte-Replenishing Ah-Scale Zinc Metal Pouch Cells With Aqueous Gel Electrolyte," *Nature Communications* 14, no. 1 (2023): 4211.

36. C. Fu, Y. Wang, C. Lu, et al., "Modulation of Hydrogel Electrolyte Enabling Stable Zinc Metal Anode," *Energy Storage Materials* 51 (2022): 588–598.

37. H. Zheng, Y. Huang, L. Zhao, et al., "Eco-Friendly Lignocellulosic Gel Polymer Electrolyte for Aqueous Zinc Energy Storage Devices," *ACS Sustainable Chemistry & Engineering* 10, no. 38 (2022): 12751–12762.

38. W. Yang, W. Yang, J. Zeng, et al., "Biopolymer-Based Gel Electrolytes for Electrochemical Energy Storage: Advances and Prospects," *Progress in Materials Science* 144 (2024): 101264.

39. H. Lu, J. Hu, X. Wei, et al., "A Recyclable Biomass Electrolyte Towards Green Zinc-Ion Batteries," *Nature Communications* 14, no. 1 (2023): 4435.

40. D. Ruiz, V. F. Michel, M. Niederberger, and E. Lizundia, "Chitin Nanofibrils From Fungi for Hierarchical Gel Polymer Electrolytes for Transient Zinc-Ion Batteries With Stable Zn Electrodeposition," *Small* 19, no. 45 (2023): 2303394.

41. Q. Liu, Z. Yu, Q. Zhuang, J. K. Kim, F. Kang, and B. Zhang, "Anti-Fatigue Hydrogel Electrolyte for All-Flexible Zn-Ion Batteries," *Advanced Materials* 35, no. 36 (2023): 2300498.

42. N. Almenara, R. Gueret, A. J. Huertas-Alonso, U. T. Veettil, M. H. Sipponen, and E. Lizundia, "Lignin–Chitosan Gel Polymer Electrolytes for Stable Zn Electrodeposition," *ACS Sustainable Chemistry & Engineering* 11, no. 6 (2023): 2283–2294.

43. N. Mittal, A. Ojanguren, D. Kundu, E. Lizundia, and M. Niederberger, "Bottom-up Design of a Green and Transient Zinc-Ion Battery With Ultralong Lifespan," *Small* 19, no. 7 (2023): 2206249.

44. Y. Meng, L. Zhang, M. Peng, et al., "Developing Thermoregulatory Hydrogel Electrolyte to Overcome Thermal Runaway in Zinc-Ion Batteries," *Advanced Functional Materials* 32, no. 46 (2022): 2206653.

45. H. Peng, X. Gao, K. Sun, et al., "Physically Cross-Linked Dual-Network Hydrogel Electrolyte With High Self-Healing Behavior and Mechanical Strength for Wide-Temperature Tolerant Flexible Supercapacitor," *Chemical Engineering Journal* 422 (2021): 130353.

46. J. Yu, H. Lin, J. Peng, et al., "In Situ Construction of Ultra-Stable Zincophilic Sodium Alginate Artificial Interface Layer for Dendrite-Free Anode in Aqueous Zinc-Ion Batteries," *Electrochimica Acta* 488 (2024): 144191.

47. B. Zhang, L. Qin, Y. Fang, et al., "Tuning Zn^{2+} Coordination Tunnel by Hierarchical Gel Electrolyte for Dendrite-Free Zinc Anode," *Science Bulletin* 67, no. 9 (2022): 955–962.

48. A. Fernández-Benito, J. C. Martinez-López, M. Javad Jafari, et al., "Green and Scalable Biopolymer-Based Aqueous Polyelectrolyte Complexes for Zinc-Ion Charge Storage Devices," *ChemElectroChem* 10, no. 22 (2023): e202300327.

49. H. Dong, J. Li, S. Zhao, et al., "Investigation of a Biomass Hydrogel Electrolyte Naturally Stabilizing Cathodes for Zinc-Ion Batteries," *ACS Applied Materials & Interfaces* 13, no. 1 (2021): 745–754.

50. M. Chen, J. Chen, W. Zhou, X. Han, Y. Yao, and C. P. Wong, "Realizing an All-Round Hydrogel Electrolyte Toward Environmentally Adaptive Dendrite-Free Aqueous Zn–MnO_2 Batteries," *Advanced Materials* 33, no. 9 (2021): 2007559.

51. Q. Han, X. Chi, S. Zhang, et al., "Durable, Flexible Self-Standing Hydrogel Electrolytes Enabling High-Safety Rechargeable Solid-State Zinc Metal Batteries," *Journal of Materials Chemistry A* 6, no. 45 (2018): 23046–23054.

52. L. Luo, Y. Liu, Z. Shen, Z. Wen, S. Chen, and G. Hong, "High-Voltage and Stable Manganese Hexacyanoferrate/Zinc Batteries Using Gel Electrolytes," *ACS Applied Materials & Interfaces* 15, no. 24 (2023): 29032–29041.

53. S. Zhang, N. Yu, S. Zeng, et al., "An Adaptive and Stable Bio-Electrolyte for Rechargeable Zn-Ion Batteries," *Journal of Materials Chemistry A* 6, no. 26 (2018): 12237–12243.

54. P. Liang, K. Zhu, Y. Rao, et al., "Hydrated Calcium Vanadate Nanoribbons With a Stable Structure and Fast Ion Diffusion as a Cathode for Quasi-Solid-State Zinc-Ion Batteries," *ACS Applied Materials & Interfaces* 16, no. 19 (2024): 24723–24733.

55. P. Sun, W. Liu, D. Yang, et al., "Stable Zn Anodes Enabled by High-Modulus Agarose Gel Electrolyte With Confined Water Molecule Mobility," *Electrochimica Acta* 429 (2022): 140985.

56. Y. Tang, C. Liu, H. Zhu, et al., "Ion-Confinement Effect Enabled by Gel Electrolyte for Highly Reversible Dendrite-Free Zinc Metal Anode," *Energy Storage Materials* 27 (2020): 109–116.

57. X. Liu, H. Zhang, D. Geiger, et al., "Calcium Vanadate Sub-Microfibers as Highly Reversible Host Cathode Material for Aqueous Zinc-Ion Batteries," *Chemical Communications* 55, no. 16 (2019): 2265–2268.

58. L.-M. Zhang, C.-X. Wu, J.-Y. Huang, X.-H. Peng, P. Chen, and S.-Q. Tang, "Synthesis and Characterization of a Degradable Composite Agarose/HA Hydrogel," *Carbohydrate Polymers* 88, no. 4 (2012): 1445–1452.

59. Siddaramaiah, T. M. M. Swamy, B. Ramaraj, and J. H. Lee, "Sodium Alginate and Its Blends With Starch: Thermal and Morphological Properties," *Journal of Applied Polymer Science* 109, no. 6 (2008): 4075–4081.

60. W. Cai, X. Zhang, G. Li, and L. Chen, "Tailoring Codirectional Zn^{2+} Pathways With Biomaterials for Advanced Hydrogel Electrolytes in High-Performance Zinc Metal Batteries," *Chemical Engineering Journal* 484 (2024): 149390.

61. L. Xu, T. Meng, X. Zheng, et al., "Nanocellulose-Carboxymethylcellulose Electrolyte for Stable, High-Rate Zinc-Ion Batteries," *Advanced Functional Materials* 33, no. 27 (2023): 2302098.

62. X. Zhong, P. Tian, C. Chen, X. Meng, H. Mi, and F. Shi, "Preparation and Interface Stability of Alginate-Based Gel Polymer Electrolyte for Rechargeable Aqueous Zinc Ion Batteries," *Journal of Electroanalytical Chemistry* 927 (2022): 116968.

63. Y. Gong, B. Wang, H. Ren, et al., "Recent Advances in Structural Optimization and Surface Modification on Current Collectors for High-Performance Zinc Anode: Principles, Strategies, and Challenges," *Nano-Micro Letters* 15, no. 1 (2023): 208.

64. S. Huang, L. Hou, T. Li, Y. Jiao, and P. Wu, "Antifreezing Hydrogel Electrolyte With Ternary Hydrogen Bonding for High-Performance Zinc-Ion Batteries," *Advanced Materials* 34, no. 14 (2022): 2110140.

65. S. Wu, M. Hua, Y. Alsaid, et al., "Poly (Vinyl Alcohol) Hydrogels With Broad-Range Tunable Mechanical Properties via the Hofmeister Effect," *Advanced Materials* 33, no. 11 (2021): 2007829.

66. F. Wang, O. Borodin, T. Gao, et al., "Highly Reversible Zinc Metal Anode for Aqueous Batteries," *Nature Materials* 17, no. 6 (2018): 543–549.

67. Z. Cao, P. Zhuang, X. Zhang, M. Ye, J. Shen, and P. M. Ajayan, "Strategies for Dendrite-Free Anode in Aqueous Rechargeable Zinc Ion Batteries," *Advanced Energy Materials* 10, no. 30 (2020): 2001599.

68. A. R. Mainar, E. Iruin, L. C. Colmenares, et al., "An Overview of Progress in Electrolytes for Secondary Zinc-Air Batteries and Other Storage Systems Based on Zinc," *Journal of Energy Storage* 15 (2018): 304–328.

69. M. Chen, J. Chen, W. Zhou, X. Han, Y. Yao, and C. P. Wong, "Realizing an All-Round Hydrogel Electrolyte Toward Environmentally Adaptive Dendrite-Free Aqueous Zn–MnO_2 Batteries," *Advanced Materials* 33, no. 9 (2021): e2007559.

70. F. Wan, L. Zhang, X. Dai, X. Wang, Z. Niu, and J. Chen, "Aqueous Rechargeable Zinc/Sodium Vanadate Batteries With Enhanced Performance From Simultaneous Insertion of Dual Carriers," *Nature Communications* 9, no. 1 (2018): 1656.

71. J. Ding, Z. Du, L. Gu, et al., "Ultrafast Zn2+ Intercalation and Deintercalation in Vanadium Dioxide," *Advanced Materials* 30, no. 26 (2018): 1800762.

72. F. Wan and Z. Niu, "Design Strategies for Vanadium-Based Aqueous Zinc-Ion Batteries," *Angewandte Chemie* 131, no. 46 (2019): 16508–16517.

73. V. Soundharrajan, B. Sambandam, S. Kim, et al., "$Na_2V_6O_{16}\cdot 3H_2O$ Barnesite Nanorod: An Open Door to Display a Stable and High Energy for Aqueous Rechargeable Zn-Ion Batteries as Cathodes," *Nano Letters* 18, no. 4 (2018): 2402–2410.

74. P. He, G. Zhang, X. Liao, et al., "Sodium Ion Stabilized Vanadium Oxide Nanowire Cathode for High-Performance Zinc-Ion Batteries," *Advanced Energy Materials* 8, no. 10 (2018): 1702463.

75. M. H. Alfaruqi, V. Mathew, J. Song, et al., "Electrochemical Zinc Intercalation in Lithium Vanadium Oxide: A High-Capacity Zinc-Ion Battery Cathode," *Chemistry of Materials* 29, no. 4 (2017): 1684–1694.

76. B. Sambandam, V. Soundharrajan, S. Kim, et al., "Aqueous Rechargeable Zn-Ion Batteries: An Imperishable and High-Energy $Zn_2V_2O_7$ Nanowire Cathode Through Intercalation Regulation," *Journal of Materials Chemistry A* 6, no. 9 (2018): 3850–3856.

77. S. Chen, Y. Zhang, H. Geng, Y. Yang, X. Rui, and C. C. Li, "Zinc Ions Pillared Vanadate Cathodes by Chemical Pre-Intercalation Towards Long Cycling Life and Low-Temperature Zinc Ion Batteries," *Journal of Power Sources* 441 (2019): 227192.

78. D. Kundu, B. D. Adams, V. Duffort, S. H. Vajargah, and L. F. Nazar, "A High-Capacity and Long-Life Aqueous Rechargeable Zinc Battery Using a Metal Oxide Intercalation Cathode," *Nature Energy* 1, no. 10 (2016): 16119.

79. Y. Zhang, F. Wan, S. Huang, S. Wang, Z. Niu, and J. Chen, "A Chemically Self-Charging Aqueous Zinc-Ion Battery," *Nature Communications* 11, no. 1 (2020): 2199.

80. C. Xia, J. Guo, P. Li, X. Zhang, and H. N. Alshareef, "Highly Stable Aqueous Zinc-Ion Storage Using a Layered Calcium Vanadium Oxide Bronze Cathode," *Angewandte Chemie* 130, no. 15 (2018): 4007–4012.

81. N. Xu, X. Lian, H. Huang, Y. Ma, L. Li, and S. Peng, "$CaV_6O_{16}\cdot 3H_2O$ Nanorods as Cathode for High-Performance Aqueous Zinc-Ion Battery," *Materials Letters* 287 (2021): 129285.

82. H. Yu, M. Aakyiir, S. Xu, J. D. Whittle, D. Losic, and J. Ma, "Maximized Crystal Water Content and Charge-Shielding Effect in Layered Vanadate Render Superior Aqueous Zinc-Ion Battery," *Materials Today Energy* 21 (2021): 100757.

83. J. Wang, J. Wang, Y. Jiang, et al., "$CaV_6O_{16}\cdot 2.8\ H_2O$ With Ca^{2+} Pillar and Water Lubrication as a High-Rate and Long-Life Cathode Material for Ca-Ion Batteries," *Advanced Functional Materials* 32, no. 25 (2022): 2113030.

84. M. Yan, P. He, Y. Chen, et al., "Water-Lubricated Intercalation in $V_2O_5\cdot nH_2O$ for High-Capacity and High-Rate Aqueous Rechargeable Zinc Batteries," *Advanced Materials* 30, no. 1 (2018): 1703725.

85. L. Suo, D. Oh, Y. Lin, et al., "How Solid-Electrolyte Interphase Forms in Aqueous Electrolytes," *Journal of the American Chemical Society* 139, no. 51 (2017): 18670–18680.

Supporting Information

Additional supporting information can be found online in the Supporting Information section.

Figure S1: Rate capability test of Zn//Zn cells at 2 mA cm^{-2}, 2 mAh cm^{-2}: a) 2M $ZnSO_4$, b) SA-GPE, c) AG-GPE, which successively underwent SEM/EDX investigations. **Figure S2:** Elemental maps from EDX analysis for SA-GPE. **Figure S3:** Elemental maps from EDX analysis for AG-GPE. **Figure S4:** Elemental maps from EDX analysis for $ZnSO_4$. **Figure S5:** Drying test of the two GPE samples at ambient conditions (a), and TGA analysis of the dried residues under N_2 flux (b).